A Monte Carlo and a Continuum Study to Predict Mechanical Properties of Nanoparticle Deposits.

O. A. Ogunsola and S. H. Ehrman*†*
**Department of Chemical and Biomolecular Engineering*
University of Maryland, College Park, MD 20742

† corresponding author, sehrman@eng.umd.edu

I. INTRODUCTION

Titania nanoparticle deposits have various applications such as gas sensors[1; 2], photocatalysts [3; 4], optical filters[5], and photovoltaic electrodes [6; 7] There have been a number of experimental and simulation studies on the influence of deposit morphology on photocatalytic activity. For example, heat sintered titania films were shown to have a more homogeneous morphology and higher electrical density than pressure sintered titania films.[8] The result was attributed to the heat sintered films being well connected. Barbe et al.[7] showed that the structure of the titania films influenced the photovoltaic response of the Grätzel solar cell. A study of titania nanoparticle size on electron diffusion by Nakade et al.[9] showed that the electron diffusion coefficient increased with particle size. Hu et al's[10] experimental study of influence of particle coordination number in nanoporous titania films and the solar cell performance revealed that the presence of small pores slows down the diffusion of electrolyte, as well as that low and very high particle coordination numbers result in lower solar cell efficiency. In simulations of the microstructure of nanoparticle films, with emphasis on titania films for solar cells, Lagemaat et al.[11] showed that increasing the porosity of the film decreases the coordination number of each particle. In another simulation study, the particle connectivity within the deposit was also shown to influence electron transport in solar cells.[12] Results of Benkstein et al's[13] study on dye sensitized titania solar cells agree with Lagemaat et al on the decrease in coordination number with increase in porosity; further more, they show that the average number of particles visited by electrons increases with porosity. A Brownian dynamics simulations study of interparticle interactions on morphology of nanoparticle deposits by Kulkarni and Biswas[14] revealed that van der Waals and Coulombic interactions influence the morphologies of the nanoparticle deposits.

In the above-mentioned studies of titania deposits, the focus is mainly on how the deposit morphology affects their photocatalytic properties. Studies have shown that particle coordination number, surface area, particle size, particle connectivity and film porosity all affect electron and electrolyte transport within the solar cell. It is not far fetched to assume that these same parameters will affect the mechanical properties of the films and solar cells. With the increasing number of applications for nanostructured deposits, it will be essential to have an understanding and control of the mechanical properties of the deposits. The mechanical properties of the deposits can then be optimized for desired applications. The mechanical properties of nanoparticle deposits have been shown in a few studies to be different from the solid bulk. Ogunsola et al.[15] experimentally estimated the Young's modulus of titania films to be 2.6 ± 1.0 MPa, significantly lower than bulk values for solid titania (230 GPa). Friedlander et al.[16] characterized the nanomechanical properties of graphitic nanoparticle chain aggregates

by AFM and found the Young's modulus value for single chain aggregates to be in the range of 3.0 to 8.8 MPa with the bulk value for graphite ranging between of 2.1 to 18.6 GPa. In both cases, the experimentally determined Young's modulus values were orders of magnitude less than bulk values.

Various groups have extensively studied aggregate and deposit growth. Meakin[17] studied the growth of aggregates in which clusters combined via linear trajectories. He concluded that the fractal dimensionality of the resulting aggregate of a cluster-cluster aggregation via linear trajectories is similar to that via Brownian motion. Meakin also used an off-lattice ballistic aggregation to deposit particles on a surface. He showed that the tangent rule for the orientation of columnar microstructures was only qualitatively correct.[18] Rosner et al.[19] used a combination of deterministic and random motion to deposit particles. The height and porosity of the deposit was shown to depend on the Peclet number in a power law manner. In a like manner, Giona and Patierno[20] used the same technique as Rosner et al. to study the structural properties of particle deposits and determined that surface and topological properties of deposits are fractal in nature. Kulkarni et al.[14] used Brownian dynamics simulations to predict the morphology of nanoparticle deposits in the presence of van der Waals and coulombic interactions. Open structured deposits were generated in the presence of van der Waals interactions and increasing the electrical field strength generated more compact deposits. Simulation of aggregates is based on whether the aggregate grows by either a monomer-cluster or a cluster-cluster mechanism. The monomer or cluster moves towards another monomer or cluster via reaction-limited, ballistic or diffusion-limited motion. Different aggregates that are fractal in nature can be generated with various fractal dimensions to indicate the compactness of the aggregate.

In this paper, we simulate fractal aggregates by a monomer-cluster and diffusion-limited method. Deposition is simulated using a Monte Carlo approach in which the aggregates are randomly moved towards the substrate sequentially. An equivalent continuum method via finite element analysis is further applied on the deposit to calculate the Young's modulus of the deposit. We report results of influence of nanostructure on Young's modulus of deposits composed of titania nanoparticle aggregates.

II. SIMULATION APPROACH

A. Aggregate Simulation

The first particle in the aggregate is created by randomly choosing x and z positions and fixing the y position from a chosen distance from the substrate. A second particle is attached to the already created first particle in a random manner. Two of the Cartesian coordinates are randomly chosen via a random number generator and the third Cartesian coordinate is calculated to ensure the interparticle distance between the two particles is equal to the particle diameter. Based on the description above, the attaching particle can be attached to the created particle in 24 different ways. The other particles making up the aggregate are attached by first, randomly choosing a particle out of the already generated aggregate and secondly, attaching in the same manner used above for the second attached particle. Each aggregate generated can have identical number of particles or a range of numbers of particles. The aggregate size is defined as the number of particles in the aggregate. The average coordination number of each aggregate is calculated using the average of the particle

coordination number. To characterize the aggregates, radius of gyration, fractal dimension and fractal prefactor are determined from equations 1 and 2.

$$R_g^2 = \frac{1}{N_p \sum_i r_i^2} \tag{1}$$

where r_i represents the distance between the center of the particle and the center of mass of the aggregate.

$$N_p = k_f \left(\frac{R_g}{d_p} \right)^{D_f} \tag{2}$$

where N_p represents the number of particles in aggregate, d_p is the diameter of a particle, R_g is the radius of gyration, D_f and k_f are the fractal dimension and fractal prefactor of the aggregate respectively.

B. Deposit simulation

The growth of the deposit is by random motion of the aggregate towards the substrate. The surrounding fluid is assumed to be air and the particle concentration is dilute, so there is no interaction between aggregates until they collide on the substrate. An aggregate is generated and released from a height H above the substrate. The generated aggregate continuously moves and collision is checked for between the particles in the incoming aggregate and deposited aggregates/substrate particles. Once a collision occurs, represented by an overlap between the particles, the aggregate is said to be deposited and the overlap removed mathematically along the axis joining the particle centers of the collided particles. The motion of the aggregates is simulated on a substrate of length L and width W. When the aggregate moves out of the sidewalls of the substrate, periodic boundary conditions are applied, in which the aggregate leaving the sidewall on one side is reintroduced on the opposite sidewall. The porosity of the deposit grown was calculated on a box (approximately 6% of deposit box) inside the deposit to remove any edge effects and was defined as:

$$P = 1 - \frac{n_{actual}}{n_{possible}} \tag{3}$$

where n_{actual} is defined as the number of simulated particles in the volume and $n_{possible}$ is defined as the number of particles that can fill the volume and is given by

$$n_{possible} = \frac{volume\ of\ box}{volume\ of\ single\ particle}. \tag{4}$$

C. Continuum Finite Element Analysis

The methodology used is based on an equivalent-continuum method (ECM) developed by Odegard et al.[21] ECM is used to determine the bulk level mechanical properties of a material by combining computational chemistry and solid mechanics. Odegard et al. used the ECM method to determine mechanical properties of a nanostructured material comprised of atoms. We extend this method here to determine mechanical properties of a nanostructured material comprised of nanoparticles.

This approach represents the particles and the bonds between the particles as an equivalent mechanical pin jointed truss model. The truss model is then substituted with an equivalent-continuum model, which is representative of the nanoparticulate structure. The equivalent continuum model is strained and the Young's modulus is calculated from the strain energy and solid mechanics constitutive laws. This method is computationally fast as finite element analysis is applied on only one structure. Fig. 1 illustrates how the equivalent-continuum model is representative of the nanostructured model.

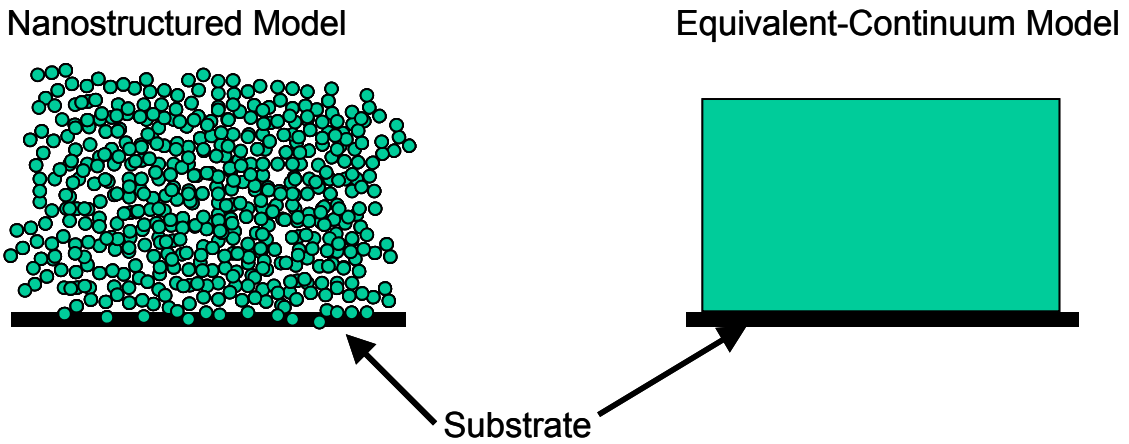

Fig. 1. Equivalent-continuum model representation of the nanoparticulate film.

In the deposit structure, it is assumed that there are only two values for the bond strengths; one representing the strong chemical bond between the particles in an aggregate and the other representing the weak Van der Waals bond strength between particles from different aggregates. This is illustrated in Fig. 2.

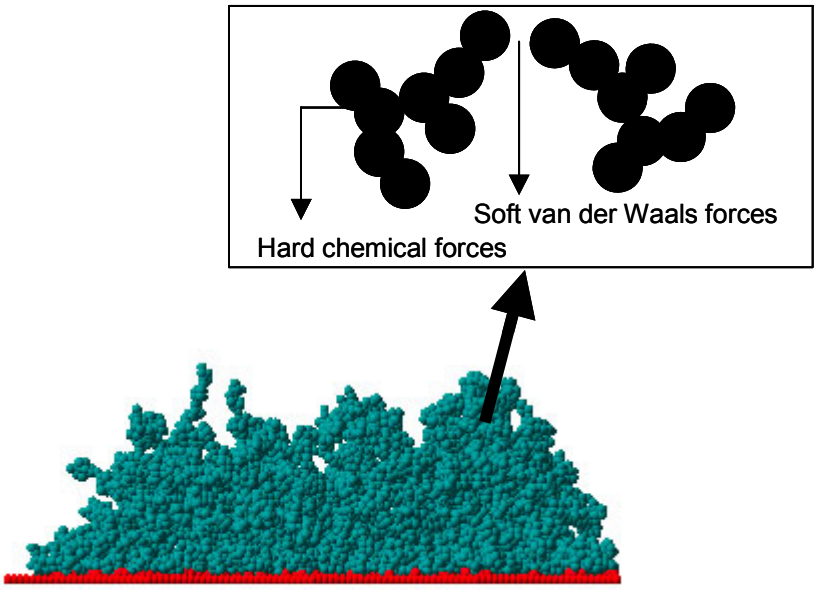

Fig. 2. Bond distribution in the nanoparticulate film.

The equivalent-continuum model involves the following:

Nanopotential Energy: The potential energy of the nanoparticulate deposit, Λ^n, is calculated as:

$$\Lambda^n = \sum E^{che} + \sum E^{vdw} \tag{5}$$

where E^{che}, defined as the chemical bond energy, is assumed to be a value that is two orders of magnitude greater than the van der Waals bond energy. This is a first approximation and is consistent with what has been reported in literature.[22] The value of chemical bond energy is assumed to change linearly with particle diameter. E^{vdw}, defined as the van der waals bond energy, is calculated from the theory of Hamaker[23] as shown in equation 6

$$E^{vdw} = -\frac{A}{12\left\{\frac{1}{x^2+2x}+\frac{1}{x^2+2x+1}+2Ln\left(\frac{x^2+2x}{x^2+2x+1}\right)\right\}} \tag{6}$$

$$x = \frac{a_o}{d_p} \tag{7}$$

where d_p is the particle diameter, a_o is an assumed interparticle distance and A, the Hamaker constant.

Equivalent Truss Model: The mechanical strain energy, Λ^t, of the pin jointed truss model in which each truss member/rod represents a chemical bond of type a or van der Waals bond of type b between the particles is calculated as shown below

$$\Lambda^t = \sum \frac{A^a E^a \left(r^a - R^a\right)^2}{2R^a} + \sum \frac{A^b E^b \left(r^b - R^b\right)^2}{2R^b} \tag{8}$$

with A^a being the cross sectional area of the rod representing a chemical bond, E^a the Young's modulus of rod a, r^a and R^a are the deformed and undeformed lengths of rod a, A^b the cross sectional area of the rod representing a van der Waals bond, E^b the Young's modulus of rod b, r^b and R^b are the deformed and undeformed lengths of rod b.

To represent the mechanical behavior of the nanoparticles with the truss model, equations 5 and 8 must be equated using the Young's modulus of each rod by introduction of the nanopotential energy into the Young's modulus. The strain energy of the truss model (equation 8) is divided into a chemical component and a van der Waals component as shown in equations 9 and 10 respectively.

$$E^{che} = \frac{A^a E^a \left(r^a - R^a\right)^2}{2R^a} \tag{9}$$

$$E^{vdw} = \frac{A^b E^b \left(r^b - R^b\right)^2}{2R^b} \tag{10}$$

An equation for the Young's modulus of the rods can be obtained by solving equations 9 and 10, for E^a & E^b as shown in equations 11 and 12.

$$E^a = \frac{2E^{che}R^a}{A^a\left(r^a - R^a\right)^2} \tag{11}$$

$$E^b = \frac{2E^{che}R^b}{A^b\left(r^b - R^b\right)^2} \tag{12}$$

The equations for Young's modulus for the rods are then replaced in the equivalent truss equation (equation 8). A finite element model is then used to calculate the resultant mechanical strain energy in the equivalent-truss structure, which is given by

$$\Lambda^t = \sum\left(E^{che}_{after\,strain} - E^{che}_{before\,strain}\right) + \left(E^{vdw}_{after\,strain} - E^{vdw}_{before\,strain}\right) \tag{13}$$

Continuum Model: the mechanical properties of the continuum (a solid rectangle as shown in Fig. 1) are determined by equating $\Lambda^t \equiv \Lambda^c$ under identical loading conditions (strain). Λ^c is the mechanical strain energy of the continuum model.

$$\Lambda^c = \frac{V\sigma_{ij}E_{ij}}{2} \tag{14}$$

where V is the volume of the rectangle, σ_{ij} is the stress component and E_{ij} is the strain component. Applying finite element analysis to the continuum structure gives

$$\Lambda^c = \pi E_L e^2 \tag{15}$$

where E_L is the longitudinal Young's modulus and e is the strain along the x-axis. Straining the truss elements changes the interparticle distance between the particles (the truss length), which results in a strain energy. The strain energies of the truss elements are calculated and summed as the mechanical strain energy of the continuum. The Young's modulus is calculated from the total strain energy and equation 15. All parameter values used are listed in Table 1.

Table I. Parameter values used in simulations.

PARAMETER	VALUES
Hamaker constant	164.9 x 10^{-21} J
Chemical bond energy	3.5 x 10^{-21} J
Strain	0.01
Chemical bond interparticle distance	0.1 nm
van der Waals bond interparticle distance	0.4 nm

III. RESULTS AND DISCUSSION

In the simulation, the fractal dimension, fractal pre-factor and average coordination number of the aggregates increased with aggregate size. The fractal dimension increased from

1.7 to 2.9. The fractal pre-factor increased from 6.2 to 9.0, while the average coordination number of the particles in each aggregate increased and stabilized at 2.02. A visual comparism of a simulated aggregate to a titania aggregate generated via an aerosol route, in Fig. 3, shows the aggregates are similar in the particles being spherical and with respect to the morphology.

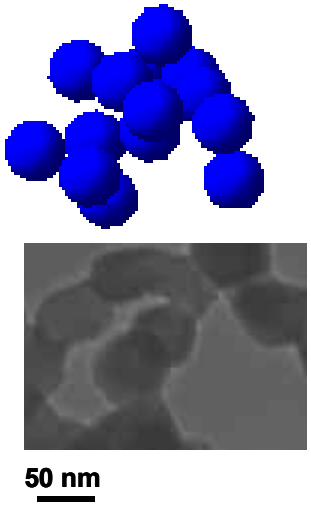

Fig. 3. Aggregate morphology generated experimentally and computationally.

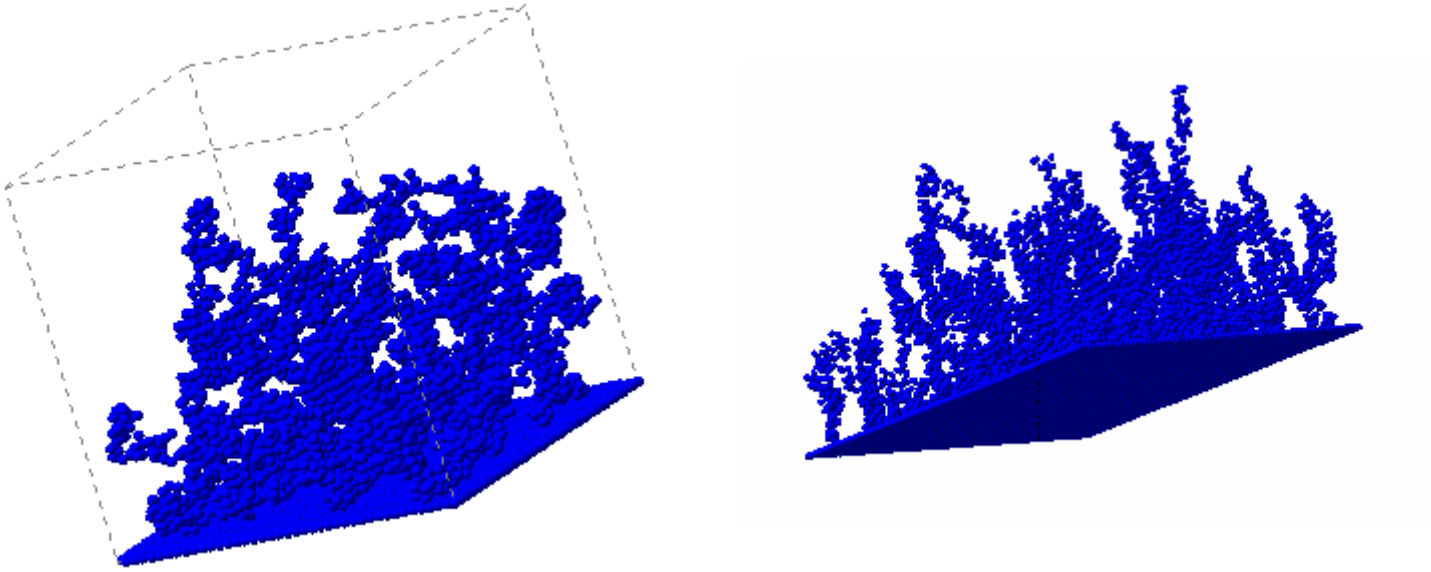

Fig. 4. Nanoparticle deposits obtained from simulation.

The deposits shown in Fig. 4 are very porous. The calculated porosity of a deposit simulated with particle size as 15 nm and aggregate size of 15 particles is 0.95, which is comparable to the 0.98 porosity of titania nanoparticle deposit experimentally deposited by Ogunsola et al.[15] The above-mentioned porous films of titania composed of nanoparticle aggregates were synthesized via gas-to-particle conversion and particle precipitated chemical vapor deposition. Indentation using atomic force microscopy, was used to determine the Young's modulus of the synthesized films. Our deposit simulations were based on achieving the same level of porosity and structure in the deposits as had been synthesized, to enable comparison of Young's modulus.

The Odegard continuum method was applied to a deposit with particle size of 15 nm, aggregate size of 15 particles and porosity of 0.95. The calculated average Young's modulus is 6.2 ± 1.4 MPa. This result was compared to Young's modulus estimated from indentation measurements of a titania deposit with similar parameters. The experimentally generated titania deposit had particles that were 17 nm in average diameter. The Young's modulus estimated from the indentation measurements was 2.6 MPa, which is comparable to the calculated Young's modulus of the simulated deposit. The very small difference is attributed to the particle size and porosity of the simulated deposit being slightly lower than the experimentally generated deposit. This shows that the continuum method is a viable way of predicting the Young's modulus of a deposit of nanoparticles. After validation of the continuum method, the effect of particle size, aggregate size and porosity on the Young's modulus was studied. Fig. 5 shows the Young's modulus of the simulated deposit increasing with decreasing particle size. This could be as a result of increase in surface energy with decreasing particle size. In a study of influence of grain size on Young's modulus, a decrease in grain size led to an increase in grain boundary defects, which ultimately resulted in a decrease in Young's modulus.[24] Our study is comparable to the results of Dinreville et al.[25] They found that the effect of surface energy on the elastic behavior becomes more significant when one of the dimensions is below 10 nm. The results of our study are comparable to the results of Dinreville et al.'s study because our simulated films are made up of particles and not grains. A reasonable explanation is that grain boundaries affect materials composed of grains, while surface energy affects materials composed of particles.

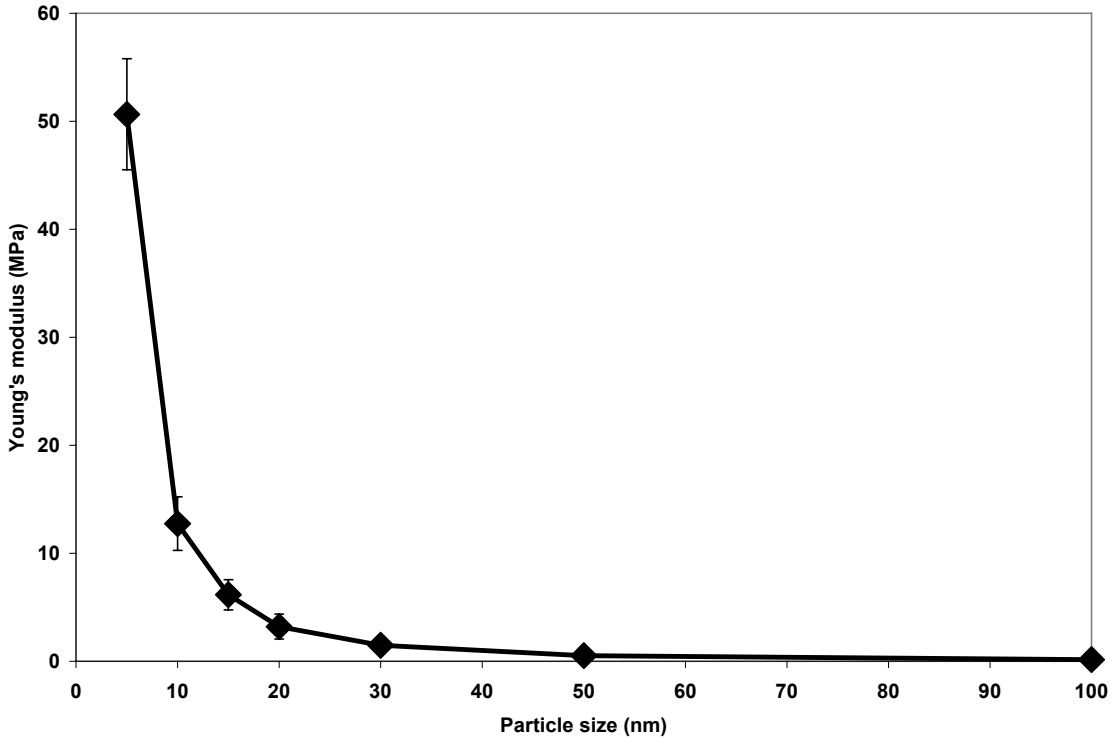

Fig. 5. Influence of particle size on Young's modulus.

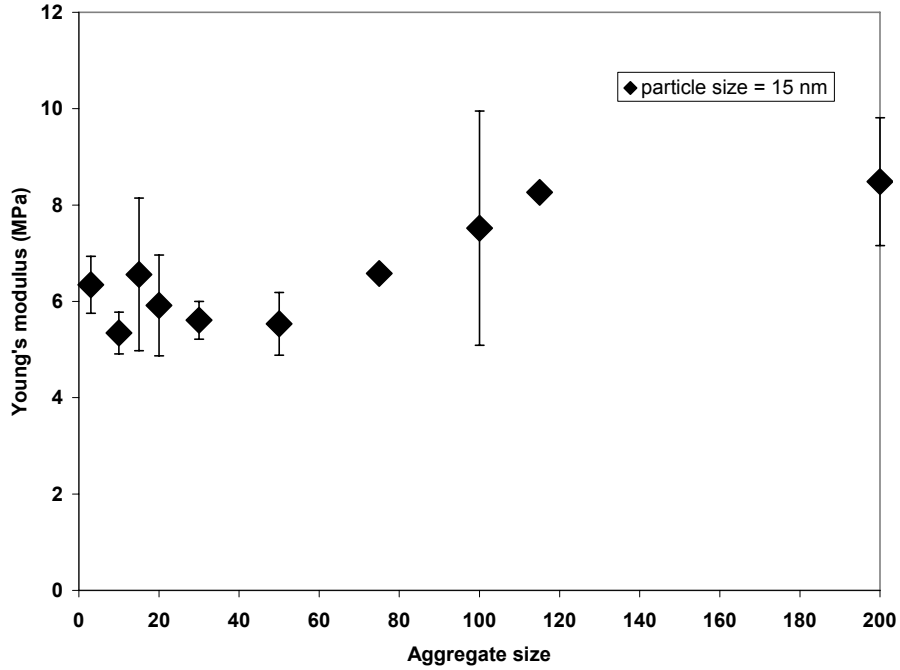

Fig. 6. Influence of aggregate size on Young's modulus.

However, our results show that aggregate size does not seem to have an effect on Young's modulus as illustrated in Fig. 6. This is perplexing, as it would be expected that increasing aggregate size would increase the chemical bonds in the deposit. It could be that at high porosities, the aggregate size effect is negligible. Young's modulus of the deposits decreased with porosity reduction as shown in Fig. 7.

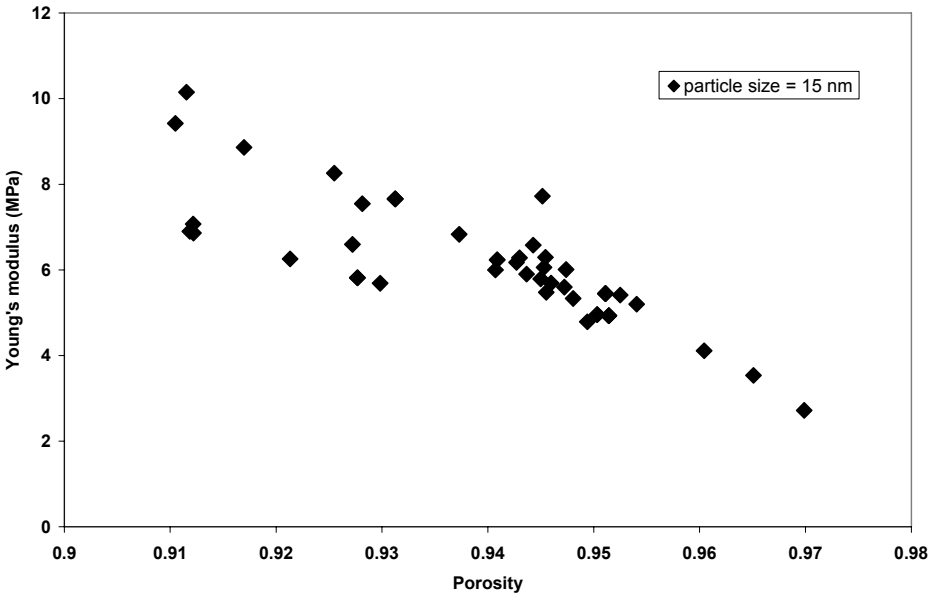

Fig. 7. Influence of porosity on Young's modulus.

Experimental[26; 27] and theoretical reports[28; 29] in the literature indicate that the young's modulus of a material reduces with increasing porosity. This makes sense as an increase in porosity corresponds to a decrease in total bond strength per volume resulting from a decrease in material.[28] This leads ultimately to a decrease in the Young's modulus.

The results of this work indicate the importance of structure (particle size and porosity) on macroscale properties such as Young's modulus.

IV. CONCLUSIONS

Aggregates were simulated via monomer-cluster diffusion limited aggregation. The simulated aggregates were deposited via Monte Carlo and a continuum method was applied to the resulting nanoparticle deposit to predict the Young's modulus of the deposit. Young's modulus of titania nanoparticle deposit of particles 15 nm in diameter and aggregate size of 15 particles was 6.2 MPa, comparable to experimental results for Young's modulus of titania nanoparticle deposits with similar parameters. Increasing particle size of nanoparticle deposit resulted in a decrease in Young's modulus. However, aggregate size had no noticeable effect on the Young's modulus. Decreasing porosity resulted in an increase in Young's modulus as expected from results reported previously in the literature.

ACKNOWLEDGEMENTS

This material is based upon work supported by the National Science Foundation under Grant No. 0093649. Any opinions, findings, and conclusions or recommendations expressed in this material are those of the authors and do not necessarily reflect the views of the National Science Foundation. O. Ogunsola acknowledges partial support through a WR Grace Fellowship.

REFERENCES

1. M. Baraton, L. Merhari, J. Wang, and K. E. Gonsalves: Investigation of the TiO_2 / PPV nanocomposite for gas sensing applications. *Nanotechnology* **9**, 356 (1998).
2. H. Tang, K. Prasad, R. Sanjines, and F. Levy: TiO_2 anatase thin films as gas sensors. *Sensors and Actuators B* **26**, 71 (1995).
3. J. Yu, and L. Chan: Photocatalytic degradation of a gaseous organic pollutant. *J. Chem. Ed.* **75**, 750 (1998).
4. Y. Ohko, K. Hashimoto, and A. Fujishima: Kinetics of photocatalytic reactions under extremely low-intensity UV illumination on titanium dioxide thin films. *J. Phy. Chem. A* **101**, 8057 (1997).
5. D. S. Hinczewski, M. Hinczewski, F. Z. Tepehan, and G. G. Tepehan: Optical filters from SiO_2 and TiO_2 multi-layers using sol-gel spin coating method. *Solar Energy Materials & Solar Cells* **87**, 181 (2005).
6. M. Grätzel, S. Y. Huang, L. Kavan, and I. Exnar: Rocking chair lithium battery based on nanocrystalline TiO_2 (anatase). *J. Electrochem. Soc.* **142**, L142 (1995).
7. C. J. Barbe, F. Arendse, P. Comte, M. Jirousek, F. Lenzmann, V. Shklover, and M. Grätzel: Nanocrystalline titanium oxide electrodes for photovoltaic applications. *J. Am. Ceram. Soc.* **80**, 3157 (1997).
8. P. D. Almeida, J. V. Deelen, C. Catry, H. Sneyers, T. Pataki, R. Andriessen, C. V. Roost, and J. Kroon: Microstructure characterization of titanium dioxide nanodispersions and thin films for dye-sensitized solar cell devices. *App. Phys. A* **79**, 1819 (2004).
9. S. Nakade, Y. Saito, W. Kubo, T. Kitamura, Y. Wada, and S. Yanagida: Influence of TiO_2 nanoparticle size on electron diffusion and recombination in dye-sensitized TiO_2 solar cells. *J. Phys. Chem. B* **107**, 8607 (2003).
10. L. Hu, S. Dai, and K. Wang: Influence of particle coordination number in nanoporous TiO_2 films on the performance of dye-sensitized solar cell modules. *Chin. Phys. Lett.* **22**, 493 (2005).
11. J. Lagemaat, K. D. Benkstein, and A. J. Frank: Relation between particle coordination number and porosity in nanoparticle films: implications to dye-sensitized solar cells. *J. Phy. Chem. B* **105**, 12433 (2001).
12. M. J. Cass, F. L. Qiu, A. B. Walker, A. C. Fisher, and L. M. Peter: Influence of grain morphology on electron transport in dye sensitized nanocrystalline solar cells. *J. Phy. Chem. B* **107**, 113 (2003).
13. K. Benkstein, N. Kopdakis, J. v. d. Lagemaat, and A. Frank: Influence of the percolation network geometry on electron transport in dye-sensitized titanium dioxide solar cells. *J. Phys. Chem. B* **107**, 7759 (2003).
14. P. Biswas, and P. Kulkarni: A Brownian dynamics simulation to predict morphology of nanoparticle deposits in the presence of interparticle interactions. *Aerosol Sci. Tech.* **38**, 541 (2004).
15. O. Ogunsola, J. Park, G. Lee, and S. Ehrman: Physical properties of porous titania films composed of nanoparticle aggregates. *Manuscript in preparation* (2005).
16. S. K. Friedlander, W. Rong, A. E. Pelling, A. Ryan, and J. K. Gimzewski: Complementary TEM and AFM force spectroscopy to characterize the nanomechanical properties of nanoparticle chain aggregates. *Nano Lett.* **4**, 2287 (2004).
17. P. Meakin: Computer simulation of cluster-cluster aggregation using linear trajectories: results from three-dimensional simulations and a comparison with aggregates formed using brownian trajectories. *J. Colloid and Interfcae Sci.* **102**, 505 (1984).
18. P. Meakin: Ballistic deposition on surfaces. *Phy. Rev. A.* **34**, 5091 (1986).
19. P. Tandon, and D. Rosner: Monte carlo simulation of particle aggregation and simultaneous restructuring. *J. Colloid and Interfcae Sci.* **213**, 273 (1999).

20. M. Giona, and O. Patierno: Monte carlo simulation of aggregation processes. *Chem. Eng. Comm.* **121**, 219 (1993).
21. G. Odegard, T. Gates, L. Nicholson, and K. Wise: Equivalent-continuum modeling of nano-structured materials. *Comp. Sci. Tech.* **62**, 1869 (2002).
22. S. Froeschke, S. Kohler, A. P. Weber, and G. Kasper: Impact fragmentation of nanoparticle agglomerates. *Aerosol Sci.* **34**, 275 (2003).
23. H. C. Hamaker: The London-Van der Waals attraction between spherical particles. *Physica* **4**, 1058 (1937).
24. A. Latapie, and D. Farkas: Effect of grain size on the elastic properties of nanocrystalline alpha iron. *Scripta Materiala* **48**, 611 (2003).
25. R. Dingreville, J. Qu, and M. Cherkaoui: Surface free energy and its effect on the elastic behavior of nano-sized particles, wires and films. *J. Mech. & Phy. Solids* **53**, 1827 (2005).
26. T. Woignier, J. Reynes, A. Alaoui, I. Beurroies, and J. Phalippou: Different kinds of structure in aerogels: relationships with the mechanical properties. *J. Non-Cryst. Solids* **241**, 45 (1998).
27. M. Moner-Girona, A. Roig, E. Molins, E. Martinez, and J. Esteve: Micromechanical properties of silica aerogels. *App. Phys. Lett.* **75**, 653 (1999).
28. H. Ma, J. Prevost, R. Jullien, and G. Scherer: Computer simulation of mechanical structure-property relationship of aerogels. *J. Non-Cryst. Solids* **285**, 216 (2001).
29. A. P. Roberts, and E. J. Garboczi: Elastic properties of model random three-dimensional open-cell solids. *J. Mech. & Phy. Solids* **50**, 33 (2002).